SUPPORTING INFORMATION

Modulation of Fe^{II} spin crossover effect in the pentadecanuclear $\{Fe_9[M(CN)_8]_6\}$ (M = Re, W) clusters by facial coordination of tridentate polyamine ligand

Szymon Chorazy,[ab] Jan J. Stanek[c], Jedrzej Kobylarczyk,[a] Shin-ichi Ohkoshi,[b] Barbara Sieklucka,[a] and Robert Podgajny*[a]*

[a]*Faculty of Chemistry, Jagiellonian University, Ingardena 3, 30-060 Krakow, Poland.*

[b]*Department of Chemistry, School of Science, The University of Tokyo, 7-3-1 Hongo, Bunkyo-ku, Tokyo, 113-0033, Japan.*

*Corresponding authors: robert.podgajny@uj.edu.pl; simon.chorazy@uj.edu.pl

Table S1 Crystal data and structure refinement for $\mathbf{1}^{HT}$, $\mathbf{1}^{LT}$, $\mathbf{2}^{HT}$, and $\mathbf{2}^{LT}$

compound		$\mathbf{1}^{HT}$	$\mathbf{1}^{LT}$	$\mathbf{2}^{HT}$	$\mathbf{2}^{LT}$
method		single-crystal XRD			
formula		$Fe_9Re_6C_{134}H_{168}N_{72}O_{14}$		$Fe_9W_6C_{134}H_{168}N_{72}O_{14}$	
formula weight [g·mol^{-1}]		4631.24		4617.14	
T [K]		240(2)	100(2)	240(2)	100(2)
λ [Å]		0.71075 (Mo Kα)		0.71075 (Mo Kα)	
crystal system		triclinic	triclinic	triclinic	triclinic
space group		P -1	P -1	P -1	P -1
unit cell	$\boldsymbol{a}$ [Å]	17.7888(10)	17.5772(9)	17.7127(4)	17.4977(4)
	$\boldsymbol{b}$ [Å]	17.8583(9)	17.6464(8)	17.7306(5)	17.5419(4)
	$\boldsymbol{c}$ [Å]	29.8019(15)	28.8773(13)	30.4366(8)	29.9576(6)
	$\boldsymbol{\alpha}$ [deg]	86.306(6)	86.341(6)	86.279(6)	86.401(6)
	$\boldsymbol{\beta}$ [deg]	81.543(6)	83.480(6)	80.322(6)	81.268(6)
	$\boldsymbol{\gamma}$ [deg]	86.298(6)	86.361(6)	86.230(6)	86.248(6)
V [Å^3]		9330.2(9)	8866.6(7)	9388.3(5)	9056.2(4)
Z		2	2	2	2
calculated density [g·cm^{-3}]		1.648	1.735	1.633	1.693
absorption coeff.[cm^{-1}]		4.620	4.861	4.400	4.561
F(000)		4544	4544	4532	4532
crystal size [mm×mm×mm]		0.15 × 0.13 × 0.07		0.18 × 0.16 × 0.09	
Θ range [deg]		2.983–27.485	2.986–25.028	2.994–27.484	3.029–27.477
limiting indices		-23 < h < 23 -23 < k < 23 -38 < l < 38	-20 < h < 20 -20 < k < 20 -34 < l < 34	-20 < h < 22 -22 < k < 23 -39 < l < 39	-20 < h < 22 -22 < k < 22 -38 < l < 38
collected reflections		131849	72887	90102	86861
unique reflections		42141	30077	42369	40971
R_{int}		0.1656	0.1474	0.0511	0.0442
completeness [%]		99.5	96.1	99.2	99.4
max. and min. transmission		0.544 and 0.738	0.529 and 0.727	0.505 and 0.693	0.494 and 0.684
refinement method		full-matrix least-squares on F^2			
data/restraints/parameters		42141/250/2067	30077/743/2071	42369/33/2067	40971/31/2067
GOF on F^2		1.203	1.273	1.446	1.178
final R indices		R_1 = 0.1697 [I>2σ(I)] wR_2 = 0.2998 (all)	R_1 = 0.2070 [I>2σ(I)] wR_2 = 0.3702 (all)	R_1 = 0.0699 [I>2σ(I)] wR_2 = 0.1388 (all)	R_1 = 0.0714 [I>2σ(I)] wR_2 = 0.1587 (all)
largest diff peak and hole		2.385 and -1.200 e·A^{-3}	3.113 and -1.584 e·A^{-3}	1.880 and -0.858 e·A^{-3}	3.437 and -1.584 e·A^{-3}

Table S2 Detailed structure parameters for $\mathbf{1}^{HT}$, $\mathbf{1}^{LT}$, $\mathbf{2}^{HT}$, and $\mathbf{2}^{LT}$ (Fe-N distances in clusters of type A)

distance [Å]	$\mathbf{1}^{HT}$	$\mathbf{1}^{LT}$	$\mathbf{2}^{HT}$	$\mathbf{2}^{LT}$
Fe1-N1	1.946(14)	1.92(2)	1.901(6)	1.892(8)
Fe1-N9	1.918(16)	1.89(3)	1.896(7)	1.892(8)
Fe1-N17	1.941(18)	1.94(3)	1.908(6)	1.895(7)
average Fe1-N	***1.935***	***1.917 (0.93%↓)[a]***	***1.902***	***1.893 (0.47%↓)[a]***
Fe2-N2	2.02(2)	1.935(17)	1.960(9)	1.962(10)
Fe2-N10	2.04(2)	1.99(3)	1.976(8)	1.951(9)
Fe2-N20	2.02(2)	1.98(3)	1.952(7)	1.915(10)
Fe2-N49	2.10(2)	2.00(5)	2.078(9)	2.050(10)
Fe2-N50	2.16(2)	2.11(4)	2.072(8)	2.031(10)
Fe2-N51	2.11(2)	2.07(3)	2.067(8)	2.057(9)
average Fe2-N	***2.075***	***2.014 (2.94%↓)***	***2.018***	***1.994 (1.19%↓)***
Fe3-N4	1.94(2)	1.95(3)	1.937(8)	1.937(4)
Fe3-N11	1.94(2)	1.85(3)	1.913(8)	1.935(11)
Fe3-N21	1.967(18)	1.92(2)	1.928(8)	1.940(10)
Fe3-N52	2.04(2)	2.07(3)	2.020(8)	2.020(10)
Fe3-N53	2.05(2)	2.06(3)	2.036(8)	2.034(9)
Fe3-N54	2.01(3)	1.95(3)	2.027(9)	2.029(11)
average Fe3-N	***1.991***	***1.967 (1.21%↓)***	***1.979***	***1.980 (0.05%↑)***
Fe4-N5	2.01(2)	2.02(4)	1.962(8)	1.932(9)
Fe4-N12	2.08(2)	2.10(3)	2.020(8)	1.966(9)
Fe4-N19	2.096(19)	2.07(3)	1.979(8)	1.942(9)
Fe4-N55	2.13(3)	2.07(4)	2.078(9)	2.045(10)
Fe4-N56	2.12(3)	2.07(5)	2.070(9)	2.038(10)
Fe4-N57	2.15(3)	2.12(4)	2.072(10)	2.061(10)
average Fe4-N	***2.098***	***2.075 (1.10%↓)***	***2.031***	***1.997 (1.67%↓)***
Fe5-N3	2.03(2)	1.96(3)	1.947(8)	1.927(8)
Fe5-N15	2.03(12)	1.96(3)	1.964(8)	1.938(8)
Fe5-N18	2.09(2)	2.04(3)	1.993(9)	1.973(10)
Fe5-N58	2.17(2)	2.10(3)	2.078(9)	2.029(10)
Fe5-N59	2.15(3)	2.10(5)	2.058(9)	2.042(10)
Fe5-N60	2.16(2)	2.10(3)	2.063(8)	2.032(9)
average Fe5-N	***2.105***	***2.043 (2.95%↓)***	***2.018***	***1.990 (1.39%↓)***
average Fe-N	***2.052***	***2.013 (1.90%↓)***	***2.001***	***1.979 (1.10↓)***

[a]- the relative change in comparison to the respective HT phase

Table S3 Detailed structure parameters for $\mathbf{1}^{HT}$, $\mathbf{1}^{LT}$, $\mathbf{2}^{HT}$, and $\mathbf{2}^{LT}$ (Fe-N distances in clusters of type B)

distance [Å]	$\mathbf{1}^{HT}$	$\mathbf{1}^{LT}$	$\mathbf{2}^{HT}$	$\mathbf{2}^{LT}$
Fe6-N25	1.935(19)	1.90(2)	1.897(6)	1.902(7)
Fe6-N33	1.93(2)	1.95(2)	1.895(7)	1.884(8)
Fe6-N41	1.916(18)	1.87(3)	1.907(7)	1.896(7)
average Fe6-N	***1.927***	***1.907 (1.04%↓)[a]***	***1.900***	***1.894 (0.32%↓)[a]***
Fe7-N27	2.07(2)	2.13(3)	2.010(9)	1.963(10)
Fe7-N35	2.13(2)	2.07(3)	2.012(9)	1.950(9)
Fe7-N42	2.09(3)	2.08(3)	2.002(10)	1.938(11)
Fe7-N61	2.12(2)	2.06(6)	2.095(11)	2.042(11)
Fe7-N62	2.13(3)	2.15(5)	2.093(10)	2.046(10)
Fe7-N63	2.13(3)	2.09(4)	2.094(12)	2.049(11)
average Fe7-N	***2.112***	***2.097 (0.71%↓)***	***2.051***	***1.998 (2.58%↓)***
Fe8-N28	1.97(2)	1.91(3)	1.923(8)	1.915(9)
Fe8-N34	2.01(2)	1.97(3)	1.923(8)	1.940(8)
Fe8-N45	1.99(2)	2.01(3)	1.946(10)	1.939(10)
Fe8-N64	2.07(3)	2.00(4)	2.039(10)	2.047(10)
Fe8-N65	2.11(2)	2.12(4)	2.054(8)	2.045(9)
Fe8-N66	2.11(2)	2.11(3)	2.043(8)	2.048(9)
average Fe8-N	***2.043***	***2.019 (1.18%↓)***	***1.988***	***1.989 (0.05%↑)***
Fe9-N26	1.969(19)	1.94(3)	1.942(7)	1.940(8)
Fe9-N37	2.02(2)	1.95(3)	1.953(9)	1.942(9)
Fe9-N43	1.98(2)	1.97(3)	1.968(8)	1.952(8)
Fe9-N67	2.05(2)	2.03(3)	2.041(8)	2.027(9)
Fe9-N68	2.05(2)	2.04(4)	2.045(9)	2.036(9)
Fe9-N69	2.07(2)	2.08(3)	2.048(7)	2.039(8)
average Fe9-N	***2.023***	***2.000 (1.14%↓)***	***2.001***	***1.989 (0.55%↓)***
Fe10-N31	2.06(2)	1.82(4)	1.946(9)	1.926(9)
Fe10-N36	2.05(2)	1.98(3)	1.955(8)	1.940(8)
Fe10-N44	2.05(2)	2.00(3)	1.940(7)	1.922(8)
Fe10-N70	2.14(3)	2.08(4)	2.048(9)	2.033(10)
Fe10-N71	2.15(2)	2.11(4)	2.064(8)	2.047(9)
Fe10-N72	2.08(2)	2.05(3)	2.042(8)	2.026(8)
average Fe10-N	***2.088***	***2.001 (4.17%↓)***	***2.000***	***1.982 (0.90%↓)***
average Fe-N	***2.051***	***2.016 (1.71%↓)***	***2.000***	***1.979 (1.06↓)***

[a]- the relative change in comparison to the respective HT phase

Table S4 Detailed structure parameters for $\mathbf{1}^{HT}$, $\mathbf{1}^{LT}$, $\mathbf{2}^{HT}$, and $\mathbf{2}^{LT}$ (C-N-Fe angles)

angle [deg]	$\mathbf{1}^{HT}$	$\mathbf{1}^{LT}$	$\mathbf{2}^{HT}$	$\mathbf{2}^{LT}$
cluster A				
C1-N1-Fe1	175.7(16)	179(2)	177.5(7)	177.8(8)
C9-N9-Fe1	178.3(18)	178(3)	179.0(7)	179.1(8)
C17-N17-Fe1	175.6(18)	174(3)	178.1(7)	177.8(8)
C2-N2-Fe2	169(2)	171(3)	176.1(8)	175.3(9)
C10-N10-Fe2	171(2)	168(3)	175.1(8)	175.9(9)
C20-N20-Fe2	176(2)	175(3)	176.8(7)	177.4(9)
C4-N4-Fe3	178(3)	177(3)	179.4(9)	178.7(10)
C11-N11-Fe3	178(2)	177(3)	177.2(7)	178.4(9)
C21-N21-Fe3	179(2)	179(3)	178.1(8)	174.8(8)
C5-N5-Fe4	173(3)	171(3)	176.4(8)	178.2(9)
C12-N12-Fe4	178(2)	176(3)	176.7(8)	178.0(9)
C19-N19-Fe4	171(2)	173(4)	175.0(7)	175.8(8)
C3-N3-Fe5	175.3(19)	177(3)	178.4(8)	177.2(8)
C15-N15-Fe5	173(2)	176(4)	174.4(8)	175.7(9)
C18-N18-Fe5	173(2)	170(3)	176.7(8)	176.1(9)
cluster B				
C25-N25-Fe6	177.3(17)	179(3)	177.6(6)	177.3(8)
C33-N33-Fe6	176.8(17)	175(2)	177.6(7)	177.1(8)
C41-N41-Fe6	177.0(17)	174(3)	177.2(6)	177.5(7)
C27-N27-Fe7	168(2)	170(3)	172.9(9)	175.9(9)
C35-N35-Fe7	173(2)	175(3)	178.0(9)	178.7(9)
C42-N42-Fe7	171(2)	172(3)	173.1(8)	174.9(9)
C28-N28-Fe8	177(3)	173(3)	179.5(8)	178.7(8)
C34-N34-Fe8	176(2)	174(3)	177.5(7)	176.9(8)
C45-N45-Fe8	179(2)	177(3)	176.1(7)	176.3(8)
C26-N26-Fe9	176(2)	179(3)	179.3(8)	178.2(8)
C37-N37-Fe9	177(2)	178(2)	177.1(8)	176.4(8)
C43-N43-Fe9	178(2)	173(3)	178.7(9)	177.9(8)
C31-N31-Fe10	173(2)	174(4)	174.4(7)	175.7(8)
C36-N36-Fe10	173(2)	176(3)	175.5(7)	175.2(8)
C44-N44-Fe10	178(2)	175(3)	179.3(9)	177.7(9)

Table S5 Detailed structure parameters for $\mathbf{1}^{HT}$, $\mathbf{1}^{LT}$, $\mathbf{2}^{HT}$, and $\mathbf{2}^{LT}$ (Re/W-C and Re/W-Fe distances)

distance [Å]	$\mathbf{1}^{HT}$	$\mathbf{1}^{LT}$	$\mathbf{2}^{HT}$	$\mathbf{2}^{LT}$
cluster A				
Re1/W1-C (range)[a]	2.09 – 2.17	2.04 – 2.16	2.12 – 2.18	2.12 – 2.18
Re2/W2-C (range)	2.09 – 2.18	2.01 – 2.19	2.12 – 2.19	2.12 – 2.20
Re3/W3-C (range)	2.04 – 2.16	2.00 – 2.16	2.14 – 2.18	2.13 – 2.20
Re1/W1-Fe1	5.16	5.12	5.18	5.17
Re1/W1-Fe2	5.25	5.19	5.27	5.25
Re1/W1-Fe3	5.20	5.18	5.24	5.25
Re1/W1-Fe4	5.28	5.26	5.29	5.25
Re1/W1-Fe5	5.28	5.24	5.25	5.23
Re2/W2-Fe1	5.15	5.11	5.18	5.16
Re2/W2-Fe2	5.26	5.22	5.28	5.26
Re2/W2-Fe3	5.18	5.15	5.20	5.20
Re2/W2-Fe4	5.34	5.32	5.34	5.30
Re2/W2-Fe5	5.28	5.24	5.26	5.25
Re3/W3-Fe1	5.15	5.13	5.18	5.17
Re3/W3-Fe2	5.27	5.22	5.27	5.24
Re3/W3-Fe3	5.19	5.17	5.24	5.24
Re3/W3-Fe4	5.29	5.26	5.27	5.25
Re3/W3-Fe5	5.34	5.28	5.30	5.29
cluster B				
Re4/W4-C (range)[a]	2.06 – 2.16	2.03 – 2.16	2.14 – 2.18	2.13 – 2.18
Re5/W5-C (range)	2.03 – 2.11	2.02 – 2.11	2.15 – 2.18	2.14 – 2.18
Re6/W6-C (range)	2.04 – 2.19	2.04 – 2.19	2.15 – 2.17	2.14 – 2.19
Re4/W4-Fe6	5.15	5.11	5.17	5.15
Re4/W4-Fe7	5.33	5.30	5.32	5.27
Re4/W4-Fe8	5.23	5.20	5.23	5.23
Re4/W4-Fe9	5.22	5.19	5.26	5.25
Re4/W4-Fe10	5.27	5.21	5.26	5.25
Re5/W5-Fe6	5.14	5.12	5.18	5.17
Re5/W5-Fe7	5.38	5.34	5.32	5.26
Re5/W5-Fe8	5.21	5.19	5.23	5.23
Re5/W5-Fe9	5.23	5.19	5.27	5.27
Re5/W5-Fe10	5.29	5.22	5.27	5.26
Re6/W6-Fe6	5.17	5.13	5.18	5.17
Re6/W6-Fe7	5.32	5.27	5.30	5.24
Re6/W6-Fe8	5.23	5.20	5.24	5.25
Re6/W6-Fe9	5.21	5.20	5.28	5.25
Re6/W6-Fe10	5.29	5.24	5.26	5.27

[a]- Re-C and Re-Fe distances for $\mathbf{1}^{HT}$ and $\mathbf{1}^{LT}$, while analogous W-C and W-Fe distances for $\mathbf{2}^{HT}$ and $\mathbf{2}^{LT}$

Table S6 Results of Continuous Shape Measure Analysis for $[M^{V}(CN)_8]^{3-}$ units in $\mathbf{1}^{HT}$, $\mathbf{1}^{LT}$, $\mathbf{2}^{HT}$, and $\mathbf{2}^{LT}$

CSM parameter	$\mathbf{1}^{HT}$	$\mathbf{1}^{LT}$	$\mathbf{2}^{HT}$	$\mathbf{2}^{LT}$
Re1/W1[a] BTP-8 parameter[b]	1.284	1.669	1.269	1.573
Re1/W1 SAPR-8 parameter	2.169	2.050	2.257	2.624
Re1/W1 DD-8 parameter	**0.751**	**0.651**	**0.715**	**0.552**
Re2/W2 BTP-8 parameter	2.186	1.871	1.941	1.838
Re2/W2 SAPR-8 parameter	2.937	2.598	2.944	2.869
Re2/W2 DD-8 parameter	**0.421**	**0.615**	**0.484**	**0.470**
Re3/W3 BTP-8 parameter	1.876	2.168	1.793	1.545
Re3/W3 SAPR-8 parameter	2.695	3.461	2.909	2.647
Re3/W3 DD-8 parameter	**0.570**	**1.332**	**0.554**	**0.588**
Re4/W4 BTP-8 parameter	2.078	2.465	1.671	1.610
Re4/W4 SAPR-8 parameter	2.749	2.915	2.718	2.739
Re4/W4 DD-8 parameter	**0.486**	**0.762**	**0.528**	**0.554**
Re5/W5 BTP-8 parameter	2.265	1.826	1.494	1.392
Re5/W5 SAPR-8 parameter	2.822	2.600	2.505	2.382
Re5/W5 DD-8 parameter	**0.826**	**0.767**	**0.634**	**0.634**
Re6/W6 BTP-8 parameter	2.303	2.449	1.838	1.575
Re6/W6 SAPR-8 parameter	3.009	3.139	2.838	2.518
Re6/W6 DD-8 parameter	**0.621**	**0.535**	**0.543**	**0.613**

[a]- Re for $\mathbf{1}^{HT}$ and $\mathbf{1}^{LT}$, W for $\mathbf{2}^{HT}$ and $\mathbf{2}^{LT}$.

[b]- CSM parameters:[S1-S3]
CSM BTP-8 = the parameter related to the bicapped trigonal prism geometry (C_{2v} symmetry)
CSM SAPR-8 = the parameter related to the square antiprism (D_{4d} symmetry)
CSM DD-8 = the parameter related to the dodecahedron (D_{2d} symmetry)
CSM = 0 for the ideal geometry and the increase of CSM parameter corresponds to the increasing distortion from the ideal polyhedron.

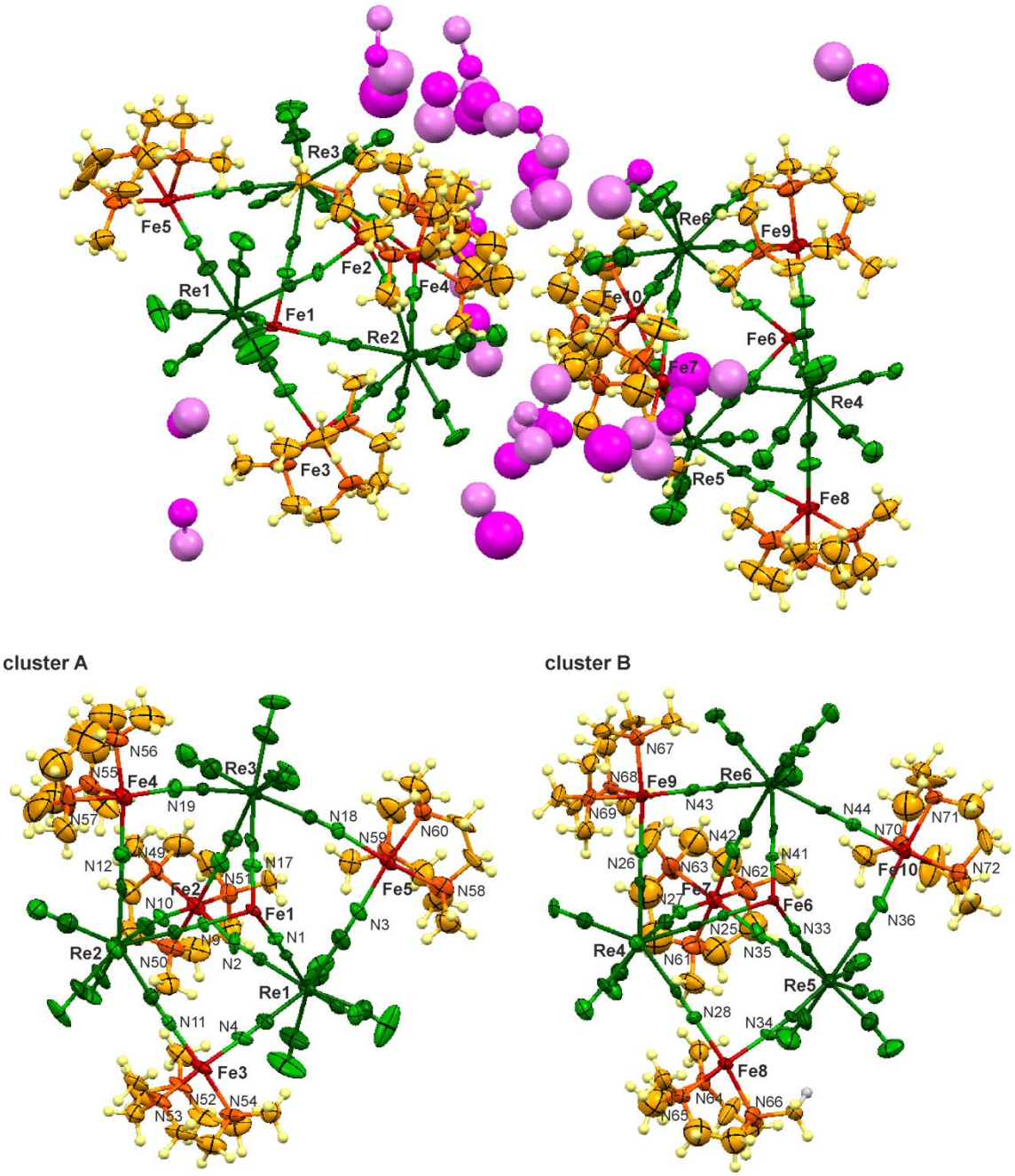

Figure S1 Asymmetric unit of **1**^{HT} with atom labelling scheme for metal ions and coordination spheres of Fe centers. Atom spheres are shown with 30% probability ellipsoids. Colours: Re, dark green; Fe, dark red; C of cyanides, green; N of cyanides, light green; N of Me_3tacn, orange, C of Me_3tacn, light orange; H, yellow; C of MeOH molecules, magenta; O of MeOH molecules, light violet.

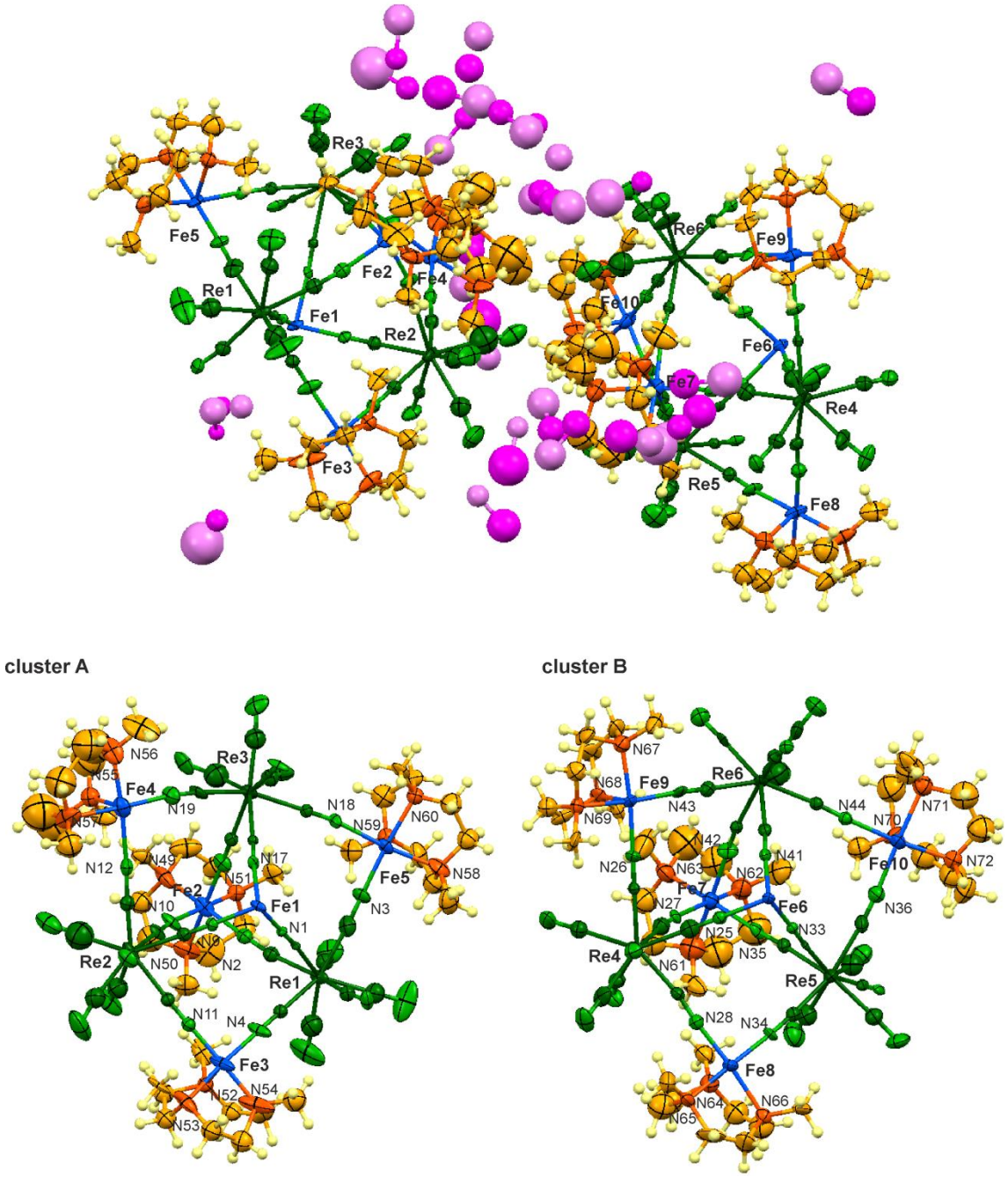

Figure S2 Asymmetric unit of $\mathbf{1}^{LT}$ with atom labelling scheme for metal ions and coordination spheres of Fe centers. Atom spheres are shown with 30% probability ellipsoids. Colours: Re, dark green; Fe, blue; C of cyanides, green; N of cyanides, light green; N of Me_3tacn, orange, C of Me_3tacn, light orange; H, yellow; C of MeOH molecules, magenta; O of MeOH molecules, light violet.

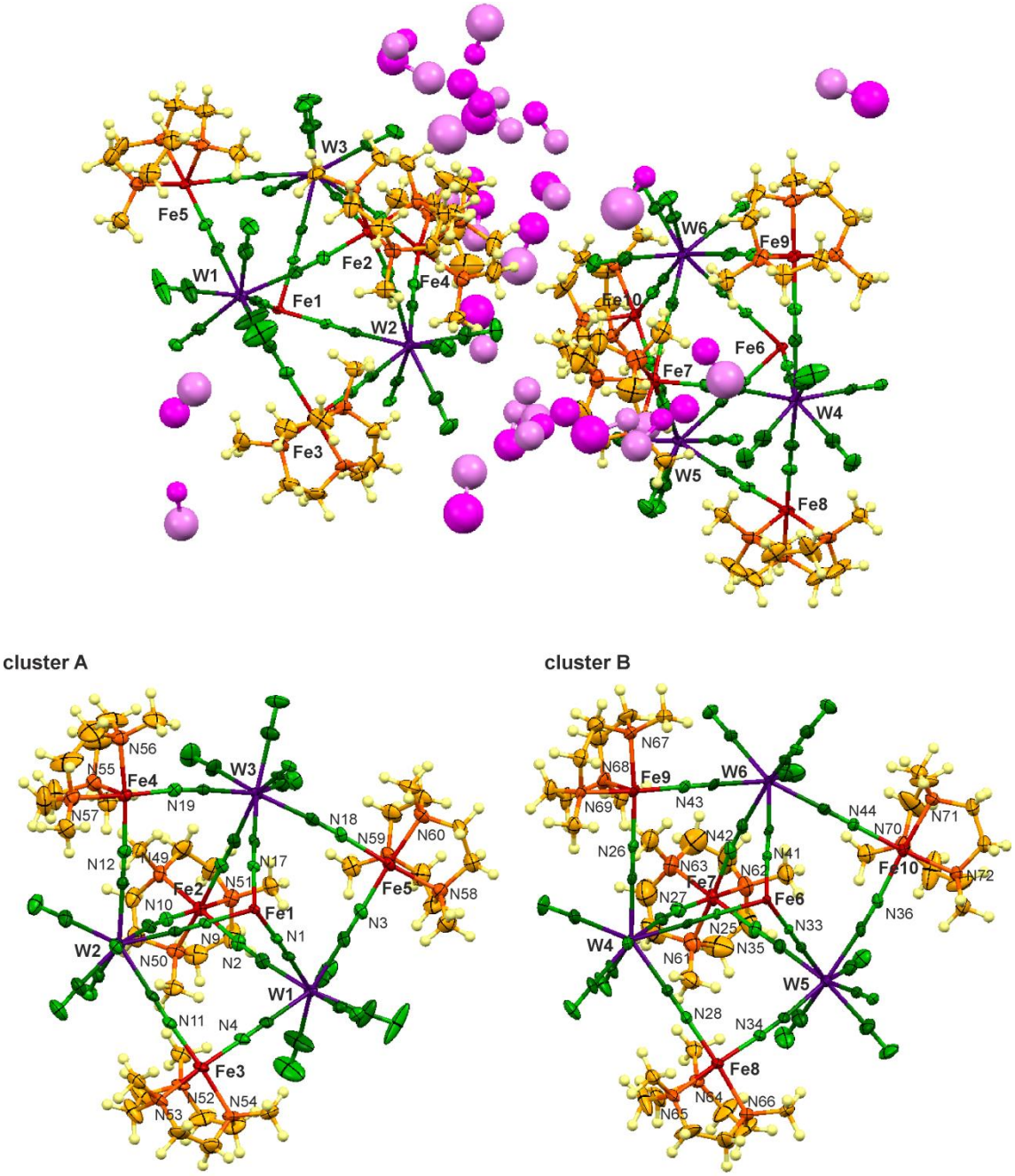

Figure S3 Asymmetric unit of $\mathbf{2^{HT}}$ with atom labelling scheme for metal ions and coordination spheres of Fe centers. Atom spheres are shown with 30% probability ellipsoids. Colours: W, dark violet; Fe, dark red; C of cyanides, green; N of cyanides, light green; N of Me_3tacn, orange, C of Me_3tacn, light orange; H, yellow; C of MeOH molecules, magenta; O of MeOH molecules, light violet.

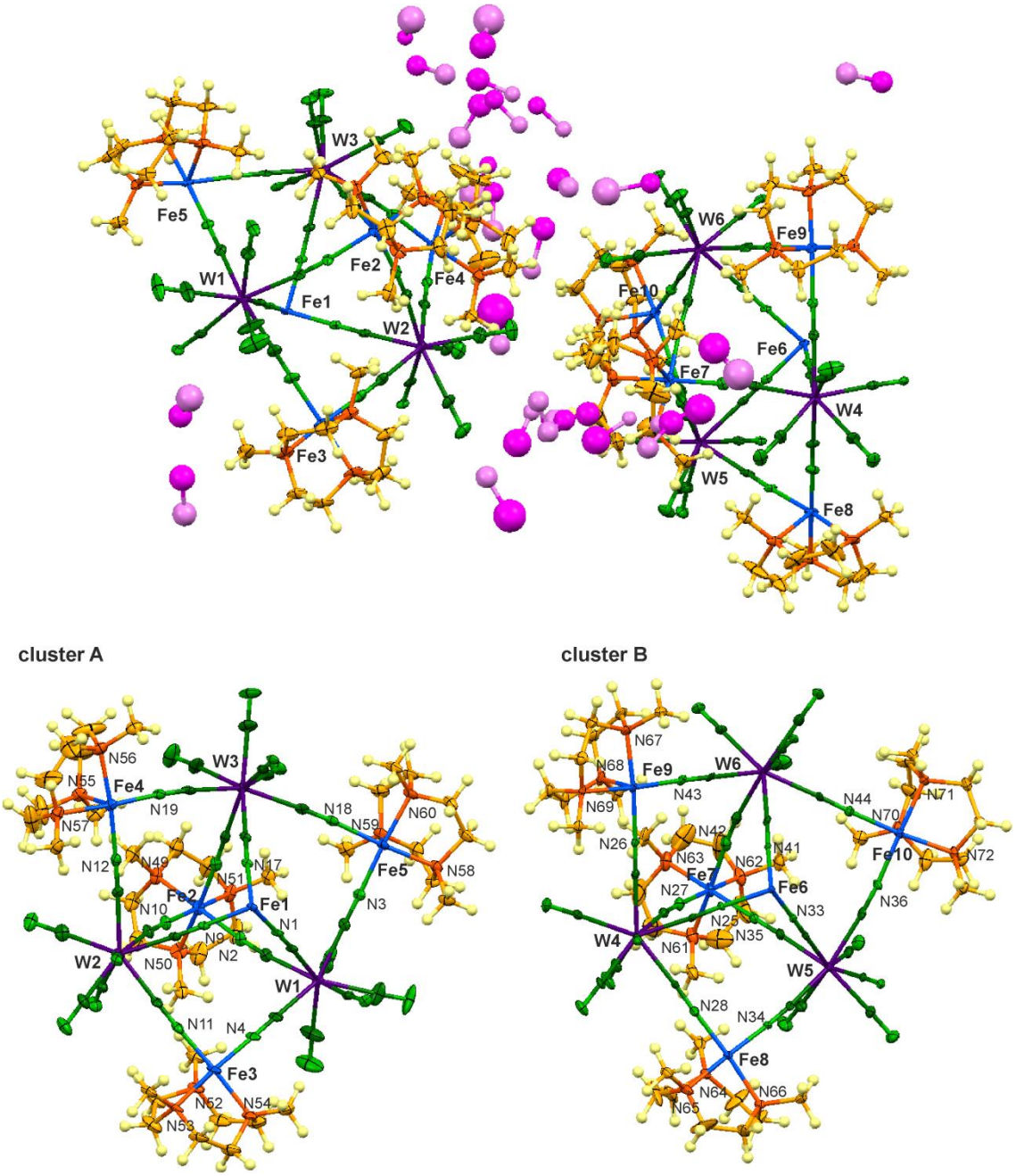

Figure S4 Asymmetric unit of $\mathbf{2}^{\mathbf{LT}}$ with atom labelling scheme for metal ions and coordination spheres of Fe centers. Atom spheres are shown with 30% probability ellipsoids. Colours: W, dark violet; Fe, blue; C of cyanides, green; N of cyanides, light green; N of Me_3tacn, orange, C of Me_3tacn, light orange; H, yellow; C of MeOH molecules, magenta; O of MeOH molecules, light violet.

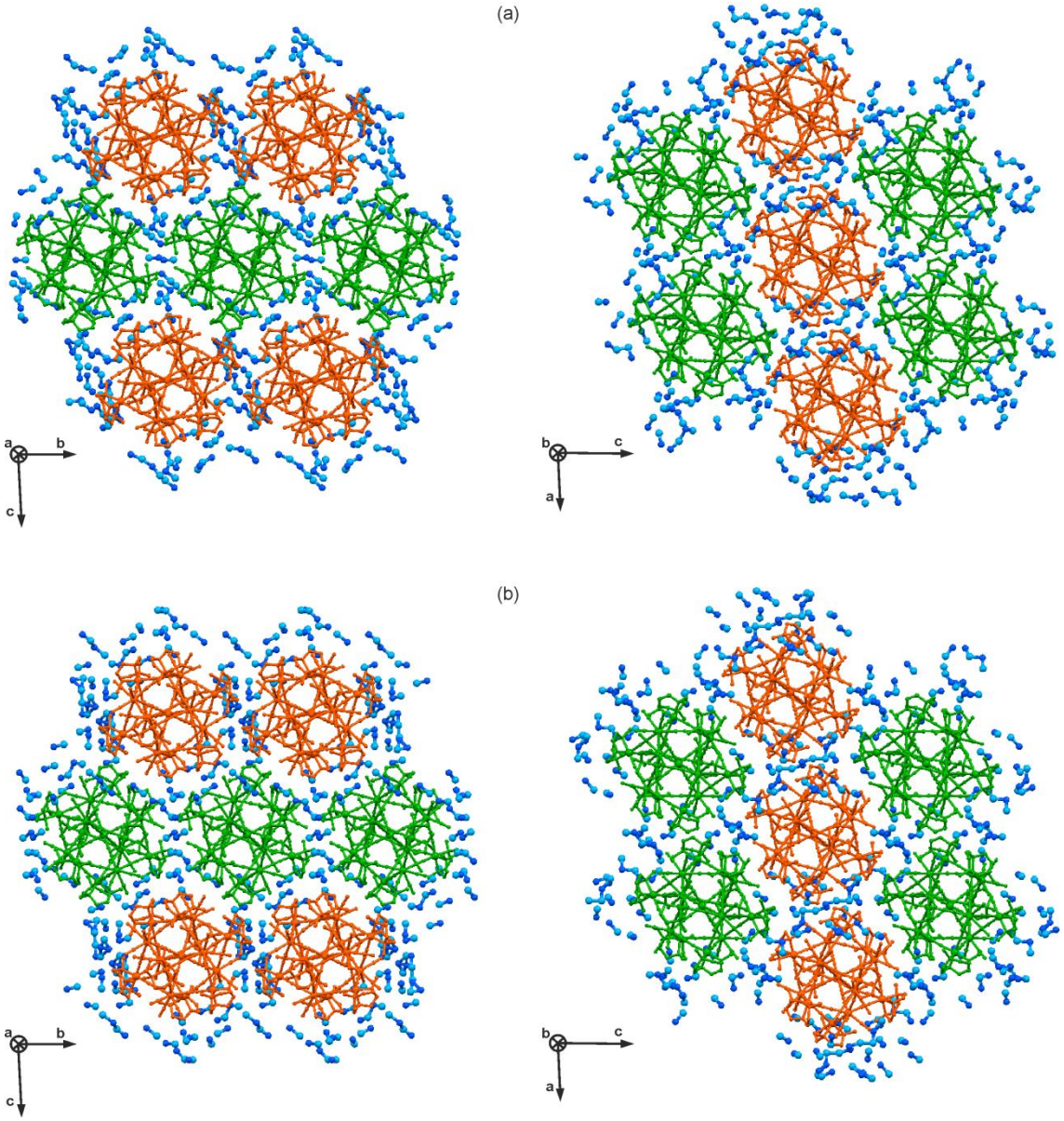

Figure S5 The supramolecular arrangement of cyanido-bridged clusters and crystallization methanol molecules of **1** (a) and **2** (b) within the *bc* (left panel) and *ac* (right panel) planes. Colours: cluster of type A, orange; cluster of type B, green; methanol, blue.

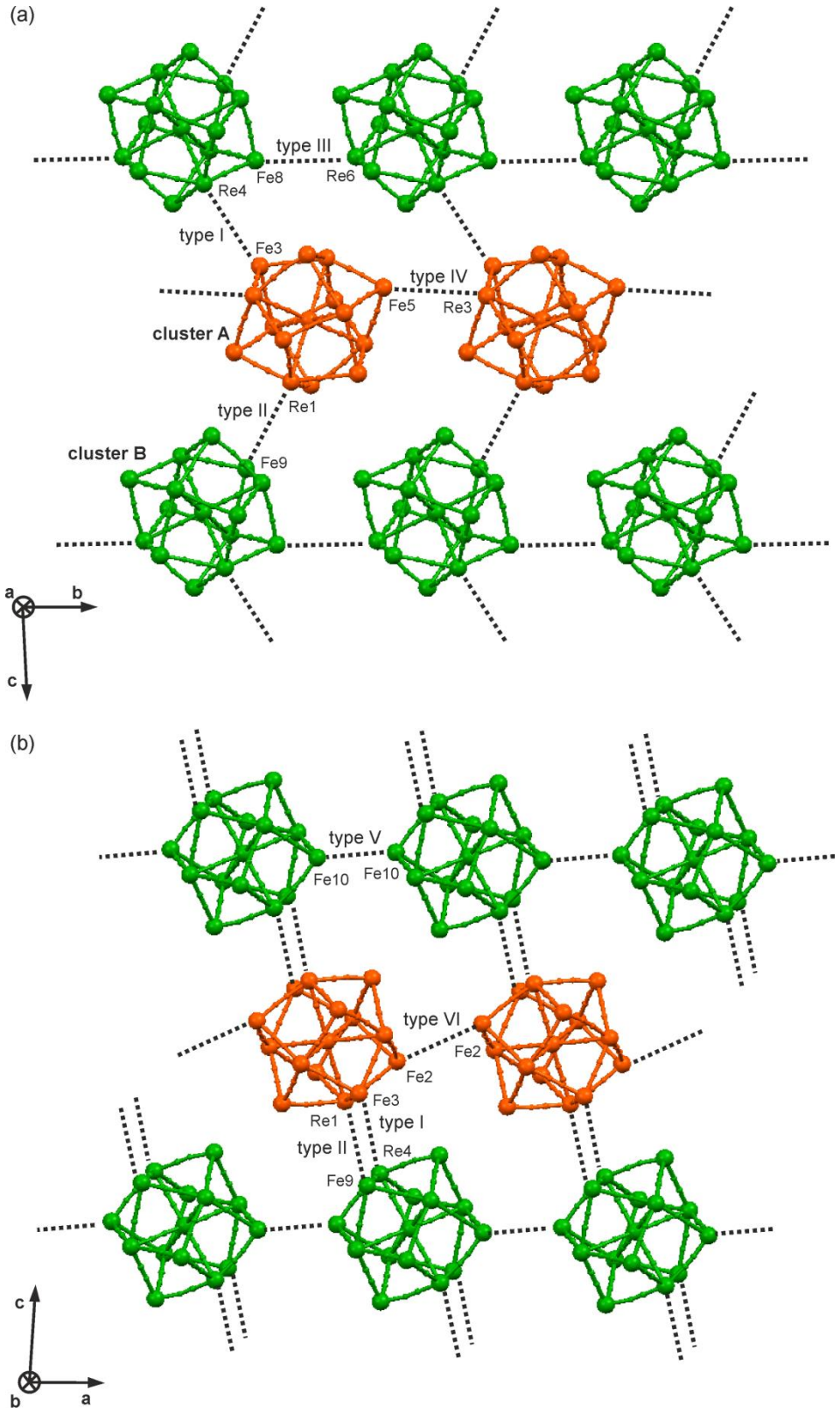

Figure S6 The supramolecular arrangement of cyanido-bridged cluster of **1** – the insight into the shortest intecluster metal–metal distances (dotted lines) presented within the *bc* (a) and *ac* (b) crystallographic planes. The six types (I-VI) of the shortest intercluster metal-metal distances (below 9 Å), and the involved atoms were labelled. Colours: cluster of type A, orange; cluster of type B. The analogous arrangement of clusters, and the analogous shortest intercluster distances were detected in **2**.

Table S7 The shortest intecluster metal–metal distances (see Figure S6) of **1** and **2** at 240(2) and 100(2) K

Distance (Figure S6)	$\mathbf{1}^{HT}$ (240 K)	$\mathbf{1}^{LT}$ (100 K)	$\mathbf{2}^{HT}$ (240 K)	$\mathbf{2}^{LT}$ (100 K)
Type I Re4/W4 – Fe3	7.800 Å	7.620 Å *(2.31%↓)*[a]	7.859 Å	7.727 Å *(1.68%↓)*
Type II Re1/W1 – Fe9	7.782 Å	7.632 Å *(1.93%↓)*	7.821 Å	7.731 Å *(1.15%↓)*
Type III Re6/W6 – Fe8	7.937 Å	7.781 Å *(1.96%↓)*	7.873 Å	7.739 Å *(1.70%↓)*
Type IV Re3/W3 – Fe5	7.959 Å	7.828 Å *(1.65%↓)*	7.846 Å	7.716 Å *(1.66%↓)*
Type V Fe10(*i*) – Fe10(*ii*)	8.458 Å	8.402 Å *(0.66%↓)*	8.431 Å	8.233 Å *(2.35%↓)*
Type VI Fe2(*i*) – Fe2(*ii*)	8.128 Å	7.903 Å *(2.77%↓)*	8.233 Å	8.050 Å *(2.22%↓)*

[a]- the relative change in comparison to the respective HT phase

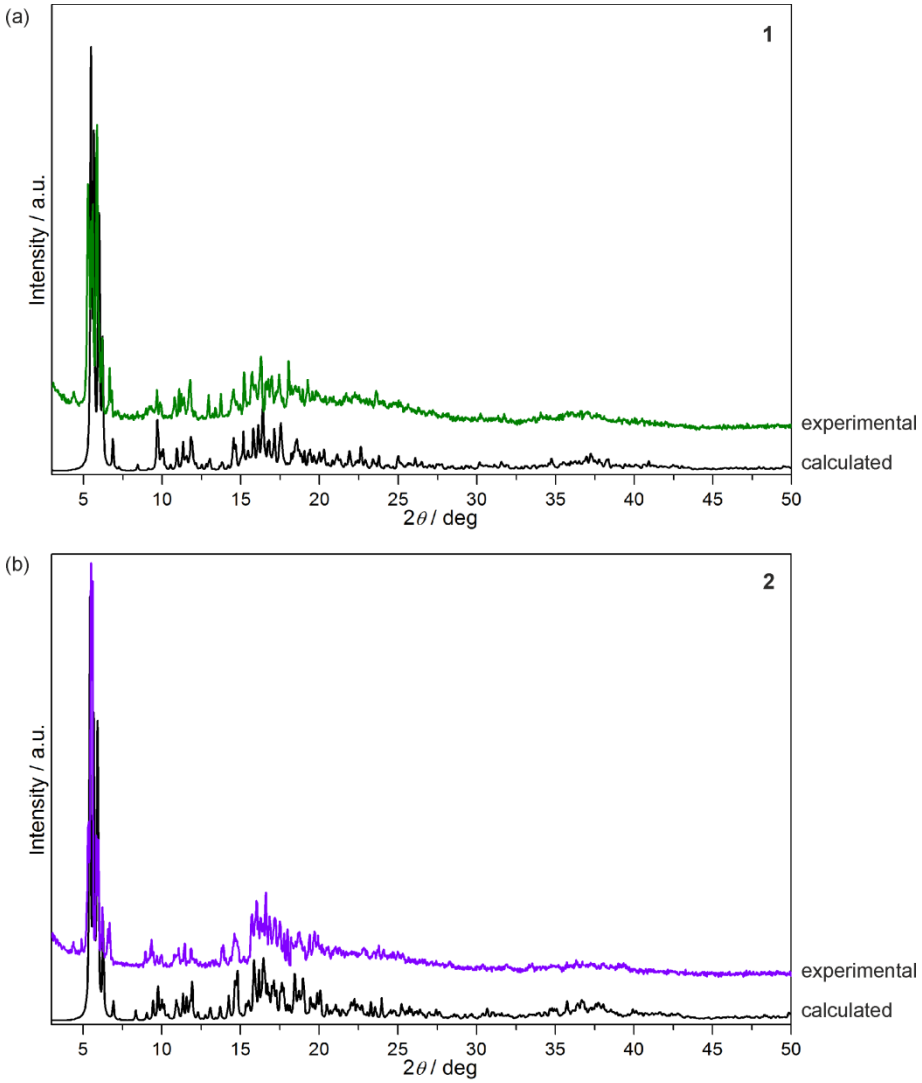

Figure S7 Experimental powder diffraction patterns of the polycrystalline samples of **1** (a) and **2** (b) compared with the calculated ones from the respective structural models obtained from the single crystal X-ray structural analyses (black lines). Only the representative ranges of 3–50° of 2Θ angle are presented. The consequent small shifts of all peaks between the experimental and the calculated patterns are due to the temperature effect related to the spin crossover phenomenon, as the powder diffraction experiments were performed at 293(2) K, while the single crystal X-ray measurements were executed at the decreased temperature of 240(2) K.

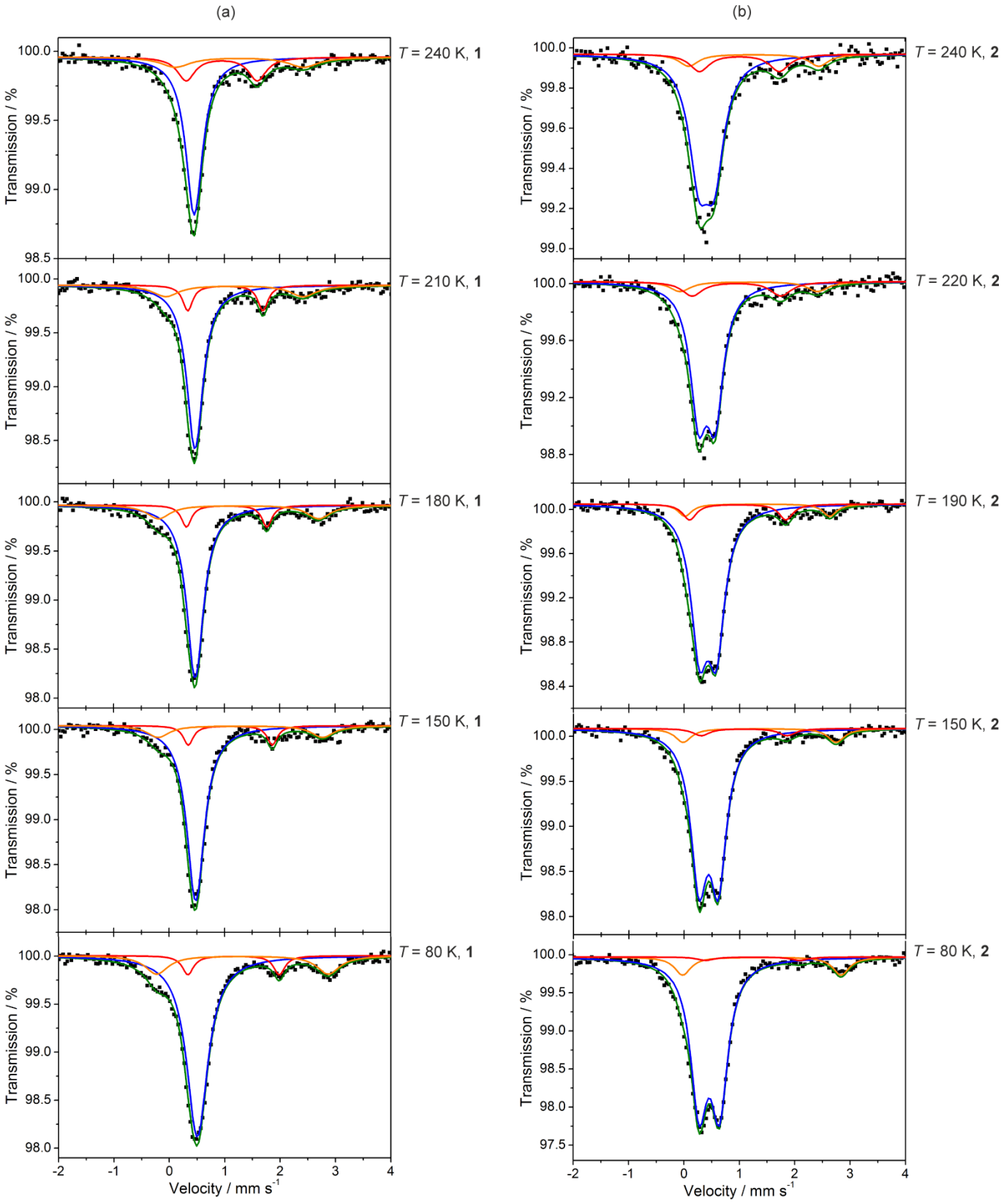

Figure S8 ^{57}Fe Mössbauer spectra of **1** (a) and **2** (b) at the indicated temperatures between 240 and 80 K. Experimental results are shown as black data points. The fitted results are presented as solid lines. Colours: $^{LS}Fe^{II}$ (blue), $^{HS}Fe^{II}$ (red and orange), total calculated fit (green).

Table S8 ^{57}Fe Mössbauer spectral parameters for **1** and **2** at the indicated temperatures.

compound	*T* / K	Fe site	isomer shift δ / mm s^{-1}	quadrupole splitting ΔE_Q / mm s^{-1}	area contribution / %
*compound **1***					
1	240(1)	LS Fe^{II}	0.45(1)	0.37(1)	64(3)
		HS Fe^{II}	0.93(2)	1.29(5)	21(3)
		HS Fe^{II}	1.25(5)	2.32(6)	15(3)
1	210(1)	LS Fe^{II}	0.45(1)	0.36(1)	71(3)
		HS Fe^{II}	1.00(1)	1.35(2)	14(3)
		HS Fe^{II}	1.17(3)	2.48(7)	15(3)
1	180(1)	LS Fe^{II}	0.45(1)	0.37(1)	73(3)
		HS Fe^{II}	1.03(1)	1.45(2)	11(3)
		HS Fe^{II}	1.24(2)	2.88(4)	16(3)
1	150(1)	LS Fe^{II}	0.46(1)	0.39(1)	77(3)
		HS Fe^{II}	1.09(1)	1.51(2)	9(3)
		HS Fe^{II}	1.27(1)	2.94(2)	14(3)
1	80(1)	LS Fe^{II}	0.49(1)	0.47(1)	75(3)
		HS Fe^{II}	1.15(1)	1.64(2)	9(3)
		HS Fe^{II}	1.30(1)	3.09(3)	16(3)
*compound **2***					
2	240(1)	LS Fe^{II}	0.38(1)	0.28(1)	70(3)
		HS Fe^{II}	0.95(2)	1.44(4)	17(3)
		HS Fe^{II}	1.23(3)	2.35(5)	13(3)
2	220(1)	LS Fe^{II}	0.37(1)	0.30(1)	80(3)
		HS Fe^{II}	0.93(2)	1.60(4)	12(3)
		HS Fe^{II}	1.18(3)	2.48(5)	8(3)
2	190(1)	LS Fe^{II}	0.38(1)	0.34(1)	86(3)
		HS Fe^{II}	1.06(2)	1.48(3)	6(3)
		HS Fe^{II}	1.30(2)	2.64(5)	8(3)
2	150(1)	LS Fe^{II}	0.40(1)	0.35(1)	87(3)
		HS Fe^{II}	1.05(2)	1.55(2)	5(3)
		HS Fe^{II}	1.34(2)	2.76(4)	8(3)
2	80(1)	LS Fe^{II}	0.42(1)	0.37(1)	88(3)
		HS Fe^{II}	1.20(2)	1.70(2)	2(2)
		HS Fe^{II}	1.37(1)	2.86(3)	10(2)

Table S9 Spin/oxidation state compositions of **1** and **2** at the selected temperatures and the related comparison between experimental and theoretical values of the molar magnetic susceptibility–temperature, $\chi_M T$ product.

compound	T / K	composition[a]	calculated $\chi_M T$ $cm^3mol^{-1}K$	experimental $\chi_M T$ $cm^3mol^{-1}K$
1	80	$(^{HS}Fe^{II})_{2.3}(^{LS}Fe^{II})_{6.7}(Re^{V})_6$	8.2[b]	8.2
	180	$(^{HS}Fe^{II})_{2.5}(^{LS}Fe^{II})_{6.5}(Re^{V})_6$	9.1	9.0
	240	$(^{HS}Fe^{II})_{3.3}(^{LS}Fe^{II})_{5.7}(Re^{V})_6$	12.0	12.8
	293	$(^{HS}Fe^{II})_{4.5}(^{LS}Fe^{II})_{4.5}(Re^{V})_6$	-	16.2
2	80	$(^{HS}Fe^{II})_{1.1}(^{LS}Fe^{II})_{7.9}(W^{V})_6$	5.9[b,c]	5.9
	190	$(^{HS}Fe^{II})_{1.3}(^{LS}Fe^{II})_{6.5}(W^{V})_6$	7.1	9.4
	240	$(^{HS}Fe^{II})_{3}(^{LS}Fe^{II})_{6}(W^{V})_6$	13.1	12.6
	293	$(^{HS}Fe^{II})_{3.8}(^{LS}Fe^{II})_{5.2}(W^{V})_6$	-	15.9

[a]the compositions for the temperatures between 80 and 240 are based on ^{57}Fe Mössbauer spectroscopy (*see* Table S8) while the composition at room temperature was estimated from the observed value of $\chi_M T$; the determination of the $^{LS}Fe^{II}$ to $^{HS}Fe^{II}$ ratio from the intensity of the corresponding quadrupole doublets (Table S8) in the Mössbauer spectra is based on the assumed proportionality between these two quantities, which neglects the thickness effects and differences in the recoil free fractions for LS and HS states of iron; these simplifications are justified by small resonant absorption effect and identical valence state of iron, respectively;

[b]the g-value of Fe(II) HS centers was estimated on the basis of the observed $\chi_M T$ product at 80 K confronted with the spin state composition taken from the ^{57}Fe Mössbauer spectroscopy at this temperature; the resulting g-value of ca. 2.2, approximately identical both for **1** and **2**, was later used for other temperatures;

[c]the W^V contribution to $\chi_M T$ product was estimated taking the parameters, $S = 1/2$ and $g = 2.0$[S4-S5];

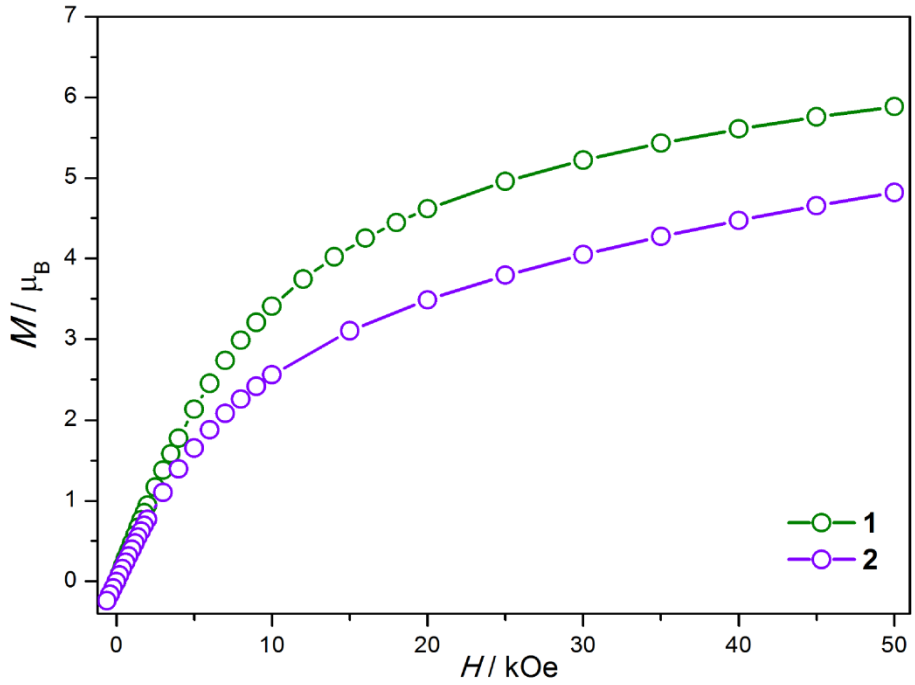

Figure S9 Field dependences of molar magnetization of **1** and **2** in the 0–50 kOe range at T = 2.0 K.

References to Supporting Information

[S1] M. Llunell, D. Casanova, J. Cirera, J. Bofill, P. Alemany, S. Alvarez, M. Pinsky and D. Avnir, *SHAPE v. 2.1. Program for the Calculation of Continuous Shape Measures of Polygonal and Polyhedral Molecular Fragments,* University of Barcelona: Barcelona, Spain, 2013.

[S2] D. Casanova, J. Cirera, M. Llunell, P. Alemany, D. Avnir and S. Alvarez, *J. Am. Chem. Soc.*, 2004, **126**, 1755.

[S3] S. Alvarez, P. Alemany, D. Casanova, J. Cirera, M. Llunell and D. Avnir, *Coord. Chem. Rev.* 2005, **249**, 1693.

[S4] N. Ozaki, H. Tokoro, Y. Hamada, A. Namai, T. Matsuda, S. Kaneko and S. Ohkoshi, *Adv. Funct. Mater.* 2012, **20**, 2089.

[S5] S. Chorazy, K. Nakabayashi, M. Arczynski, R. Pełka, S. Ohkoshi and B. Sieklucka, *Chem. Eur. J.* 2014, **20**, 7144.